

# FinGPT-HPC: Efficient Pretraining and Finetuning Large Language Models for Financial Applications with High-Performance Computing

Xiao-Yang Liu<sup>1</sup>, Jie Zhang<sup>2</sup>, Guoxuan Wang<sup>3</sup>, Weiqing Tong<sup>2</sup>, and Anwar Walid<sup>1</sup>

<sup>1</sup>Department of Electrical Engineering, Columbia University

<sup>2</sup>School of Computer Engineering and Science, Shanghai University

<sup>3</sup>Department of Computer Science, Whiting School of Engineering, Johns Hopkins University

Emails: {XL2427, aie13}@columbia.edu, {zhangjie, wqtong}@shu.edu.cn, gwang69@jhu.com

**Abstract**—Large language models (LLMs) are computationally intensive. The computation workload and the memory footprint grow quadratically with the dimension (layer width). Most of LLMs’ parameters come from the linear layers of the transformer structure and are highly redundant. These linear layers contribute more than 80% of the computation workload and 99% of the model size. To pretrain and finetune LLMs efficiently, there are three major challenges to address: 1) reducing redundancy of the linear layers; 2) reducing GPU memory footprint; 3) improving GPU utilization when using distributed training. Prior methods, such as LoRA and QLoRA, utilized low-rank matrices and quantization to reduce the number of trainable parameters and model size, respectively. However, the resulting model still consumes a large amount of GPU memory. In this paper, we present high-performance GPU-based methods that exploit low-rank structures to pretrain and finetune LLMs for financial applications. We replace one conventional linear layer of the transformer structure with two narrower linear layers, which allows us to reduce the number of parameters by several orders of magnitude. By quantizing the parameters into low precision (8-bit and 4-bit), the memory consumption of the resulting model is further reduced. Compared with existing LLMs, our methods achieve a speedup of 1.3 $\times$  and a model compression ratio of 2.64 $\times$  for pretraining without accuracy drop. For finetuning, our methods achieve an average accuracy increase of 6.3% and 24.0% in general tasks and financial tasks, respectively, and GPU memory consumption ratio of 6.3 $\times$ . The sizes of our models are smaller than 0.59 GB, allowing inference on a smartphone.

**Index Terms**—LLMs, GPUs, low-rank, high-performance computing, FinGPT

## I. INTRODUCTION

Large language models (LLMs) have achieved great success in many domains. Pretraining LLMs with hundreds of billions of parameters may take millions of GPU hours, say run 500 GPUs for 6 months. Table I provides a summary of the model size and typical training time for popular LLMs. A widely adopted approach is finetuning a pretrained LLM on private datasets. However, LLMs have a large number of parameters, and the finetuning process may still consume hundreds of gigabytes of GPU memory. Most of the parameters of LLMs, i.e.  $\geq 99\%$ , come from the linear layers of the transformer structure [1], where the computation workload and the memory footprint grow quadratically with the dimensions (i.e., layer width). For example, the dimensions of hidden layers of

TABLE I  
POPULAR LLMs: NUMBER OF PARAMETERS (BILLION), MODEL SIZE (MEMORY), DATASET (DISK), AND TRAINING TIME (GPU $\times$ HOURS).

LLMs	#Parameters	Size (GB)	Data (TB)	Training (hours)
GPT-3 [7]	175B	350	0.9	835584
Llama2 [2]	7B; 13B; 70B	14; 26; 140	4.6	184320; 368640; 1720320
Falcon [8]	7B; 40B; 180B	14; 80; 360	2.1	129024; 571392; $\sim$ 7000000
ChatGLM3 [9]	6B	12	1.3	1105920
Mistral-8 $\times$ 7B [10]	46.7B	93.4	-	-

Llama2-7B [2] and Llama2-13B [2] are 4096 and 5120, respectively, and the numbers of (decoder) layers are 32 and 40, respectively. The model size and training time of Llama2-13B is about twice that of Llama2-7B, as shown in Table I.

**Challenges.** Employing LLMs is highly computing-intensive and there are several challenges to contend with:

- The pretraining dataset is too large to fit into GPU memory (e.g., 32 GB or 80 GB) or even CPU memory (e.g., 63 GB or 128 GB), as shown in Table I. During the training process, data is loaded into GPU memory from the disk (e.g., 1 TB or 4 TB), which is time-intensive.
- LLMs require large GPU memory during both the training and inference stages (more details can be found in Table III).
- When using the model-parallel method [3] to pretrain an LLM across multiple GPUs, these GPUs remain under low utilization.

The low-rank adaptation (LoRA) method [4] is a parameter-efficient finetuning method. It utilizes the low-rank structure to reduce the redundancy of the linear layers in the transformer structure [1]. Further, the quantized LoRA (QLoRA) method [5] converts the precision of parameters from half-precision (16-bit) into INT8 (8-bit) or INT4 (4-bit), which can reduce the GPU memory consumption. The TensorGPT method [6] replaces the embedding layer with low-rank tensor-train structure to efficiently capture the weights correlations.

In this paper, we present efficient pretraining and finetuning LLMs for financial applications with high-performance computing. Our method has two parts: pretraining and finetuning, as shown in Fig. 1. First, we pretrain a low-rank LLM on a general dataset and obtain a general LLM. Second, we

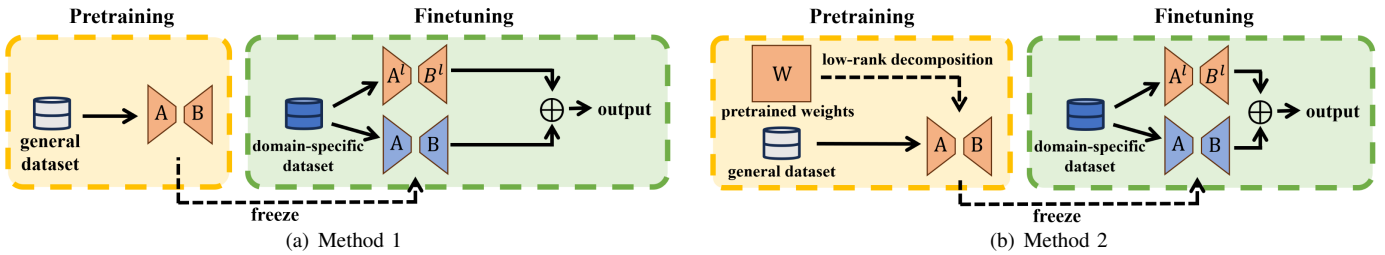


Fig. 1. Our methods for pretraining (left) and finetuning (right) LLMs. We replace a linear layer of the transformer network [1] with two linear layers with weight matrices  $A$  and  $B$ .

finetune the LLM on domain-specific datasets by freezing the pretrained weights and adding a low-rank version on a parallel path.

Our contributions can be summarized as follows.

- We provide a new training paradigm. We employ the low-rank structure and quantization technique in the linear layers of the transformer structure, leading to a substantial reduction in the number of trainable parameters. Therefore, both the GPU memory footprint and running time of both pretraining and finetuning LLMs are greatly reduced. Furthermore, the response time and memory required in the inference stage are also reduced.
- We utilize a recomputing technique to reduce the peak number of intermediate variables so that the GPU memory footprint of pretraining and finetuning LLMs are greatly reduced. Using the pipeline model-parallel method, we improve the GPU utilization in pretraining across multiple GPUs, thus reducing the pretraining time.
- We perform extensive experiments to evaluate the performance of our methods. For pretraining GPT2-1.5B [11], our method achieves a speedup of  $1.3\times$ , and our pretrained LLM has a compression ratio of  $2.64\times$  without accuracy drop. For finetuning Llama2-13B [2], our method achieves an average accuracy increase of 6.3% and 24.0% in general tasks and financial tasks, respectively, and a reduction of GPU memory footprint by  $6.3\times$ .

The remainder of this paper is organized as follows. Section II discusses related works. Section III gives a background on LLMs and the low-rank structure. Section IV presents our method for pretraining LLMs. Section V presents our method for finetuning LLMs. Section VI describes the experimental settings and results. In Section VII, we provide concluding remarks.

## II. RELATED WORKS

### A. Large Language Models (LLMs)

The transformer structure [1] uses the self-attention mechanism and allows the model to process sequential data efficiently. It performs much better in processing texts than previous neural network structures. GPT-1 [12] is one of the first generative pretrained transformer (GPT). GPT-3 [7] has significantly increased the model size from 1.5 B to 175 B.

It is the base model of ChatGPT, which was trained using instruction finetuning [13]. LLaMA [14] is an open-source pretrained LLM, which has three versions with parameter sizes of 7B, 13B and 70B, respectively.

J. Kaplan *et al.* [15] proposed the scaling law of LLMs, where the model performance scales as a power-law with model size, dataset size, and the amount of compute used for pretraining. K. Cobbe *et al.* [16] showed that the scaling law also applies to model fine-tuning. J. Wei *et al.* [17] discovered that LLMs have emergent abilities, which are not present in smaller models but are present in larger models.

### B. Low-rank Structure and Quantization Technique

**Low-rank structure.** Using the low-rank structure can greatly reduce the parameters of the linear layers. The Low-rank adaptation (LoRA) method [4] reduced the number of trainable parameters by a factor of 10,000 times. However, it still retained a full-size pretrained LLM for inference. Much research focused on decomposing pretrained models [18], and there was a significant performance drop for low-rank models [19]. Tensor layers are suited for computing on GPUs [20]–[23], and have the low-rank feature [24], [25]. H. Huang *et al.* [26] used hierarchical tucker layers to reduce the model’s accuracy drop, but incurred a longer training time. X.-Y. Liu *et al.* [27] used high-performance tucker layers to accelerate the training.

**Quantization technique.** Quantization maps high-precision data to low-precision data [28], which can effectively reduce the memory consumption. T. Dettmers *et al.* [29] implemented a selective quantization strategy. Data in the outlier vectors is kept in the original precision, while data in other vectors is quantized into int8 format. G. Xiao *et al.* [30] discovered that outliers make the activations difficult to quantize and have less impact on the weights. The authors altered the value range of activations and weights, balancing their quantitative difficulty. Besides reducing the effect of outliers, E. Frantar *et al.* [31] reduced accuracy loss by improving the rounding strategy. However, they did not use quantization in the pretraining stage.

## III. BACKGROUND ON LLMs AND LOW-RANK STRUCTURES

### A. Decoder-only Transformer Structure

Most existing LLMs are based on the decoder-only transformer structure [1]. Fig. 2 shows the structure of Llama2 [2].

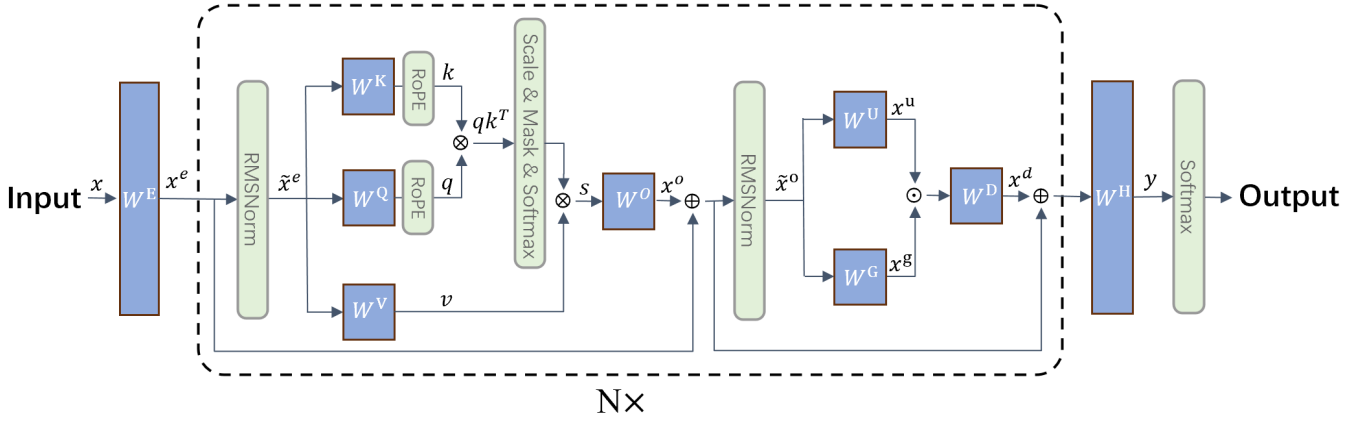


Fig. 2. The transformer structure (decoder-only) of Llama2.

TABLE II  
BREAKDOWN OF PARAMETERS IN **LLAMA2-7B** ( $N = 32$ ) AND **LLAMA2-13B** ( $N = 40$ ).

Module	Size	Amount (M)	Storage (GB)	Percentage (%)
$W^E$	$32000 \times 4096$ , $32000 \times 5120$	131.07, 163.84	0.26, 0.33	1.94, 1.25
RMSNorm	4096, 5120	0.13, 0.21	$\ll 0.01$	$\ll 0.01$
$W^Q$	$4096 \times 4096$ , $5120 \times 5120$	536.87, 1048.56	1.07, 2.10	7.98, 8.07
$W^K$	$4096 \times 4096$ , $5120 \times 5120$	536.87, 1048.56	1.07, 2.10	7.98, 8.07
$W^V$	$4096 \times 4096$ , $5120 \times 5120$	536.87, 1048.56	1.07, 2.10	7.98, 8.07
$W^O$	$4096 \times 4096$ , $5120 \times 5120$	536.87, 1048.56	1.07, 2.10	7.98, 8.07
RMSNorm	4096, 5120	0.13, 0.21	$\ll 0.01$	$\ll 0.01$
$W^U$	$4096 \times 11008$ , $5120 \times 13824$	1442.84, 2834.84	2.89, 5.67	21.40, 21.74
$W^G$	$4096 \times 11008$ , $5120 \times 13824$	1442.84, 2834.84	2.89, 5.67	21.40, 21.74
$W^D$	$11008 \times 4096$ , $5120 \times 13824$	1442.84, 2834.84	2.89, 5.67	21.40, 21.74
$W^H$	$4096 \times 32000$ , $32000 \times 5120$	1442.84, 163.84	0.26, 0.33	1.94, 1.25

It consists of three parts:

- First, there is an embedding layer that converts the input  $x$  to a latent vector  $x^e$ .
- Second, there are  $N$  decoder layers. Each decoder has two modules: the multi-head self-attention module and the feed-forward network module. The self-attention module transforms  $x^e$  to  $x^o$ . The feed-forward network module transforms  $x^o$  to  $x^d$ . In addition, the inputs  $x^e$  and  $x^o$  are skip-connected to the output  $x^o$  and  $x^d$ , respectively. For each module, there is a normalization layer that normalizes  $x^e$  and  $x^o$  to  $\tilde{x}^e$  and  $\tilde{x}^o$ , respectively.
- Finally, there is an output layer  $W^H$  that converts the latent representations  $x^d$  to  $y$ . Then, the softmax function transforms  $y$  to a vector of probabilities, where each entry is the probability of picking the corresponding token.

In the multi-head self-attention module,  $\tilde{x}^e$  is linearly projected  $h$  times with different, learned projections to  $k, q, v \in \mathbb{R}^d$ . The number of heads is  $h$ . Attention functions are performed in parallel. In the attention function,  $qk^T$  is masked and scaled by  $\frac{1}{\sqrt{d}}$  before feeding into the softmax function.

After the attention function, we get  $head_i$ ,  $i = 1, 2, \dots, h$ .

$$head_i = \text{Attention}(q, k, v) = \text{softmax}\left(\frac{qk^T}{\sqrt{d}}\right)v,$$

$$q = \text{RoPE}(W_i^Q \tilde{x}^e), \quad k = \text{RoPE}(W_i^K \tilde{x}^e), \quad v = W_i^V \tilde{x}^e, \quad (1)$$

where RoPE [32] is the Rotary Position Embedding function.

Concatenating these  $head_i$ , input to  $W^O$  and obtain  $x^o$ :

$$x^o = \text{Concat}(\text{head}_1, \dots, \text{head}_h) W^O. \quad (2)$$

The feed-forward network consists of three linear layers:

$$x^d = W^D(\underbrace{W^U \tilde{x}^o}_{x^u} \odot \text{SiLU}(\underbrace{W^G \tilde{x}^o}_{x^g})), \quad (3)$$

where SiLU is the activation function and  $\odot$  is the element-wise product.

Given an input token,  $x \in \mathbb{R}^{32000}$ , the forward processing of Fig. 2 with parameters in Table II is as follows:

- Input  $x$  to an embedding layer  $W^E \in \mathbb{R}^{32000 \times 4096}$ , we get an embedding vector  $x^e = W^E x \in \mathbb{R}^{4096}$ .
- Renormalize  $x^e \in \mathbb{R}^{4096}$  through an RMSNorm layer and

- get  $\tilde{\mathbf{x}}^e \in \mathbb{R}^{4096}$ .
- Perform products of  $\tilde{\mathbf{x}}^e$  with weight matrices  $\mathbf{W}^K \in \mathbb{R}^{4096 \times 4096}$ ,  $\mathbf{W}^Q \in \mathbb{R}^{4096 \times 4096}$ ,  $\mathbf{W}^V \in \mathbb{R}^{4096 \times 4096}$ , the results  $\mathbf{k}, \mathbf{q}, \mathbf{v} \in \mathbb{R}^{4096}$  are split into  $h = 32$  parts. Each part performs an attention function in parallel as in (1). We get  $head_i \in \mathbb{R}^{4096 \times 128}$ ,  $i = 1, 2, \dots, 32$ .
  - Concatenate these  $head_i$  and performing products with weight matrix  $\mathbf{W}^O \in \mathbb{R}^{4096 \times 4096}$ , and get  $\mathbf{x}^o \in \mathbb{R}^{4096}$  as in (2).
  - Input  $\mathbf{x}^o$  to an RMSNorm layer, we get  $\tilde{\mathbf{x}}^o \in \mathbb{R}^{4096}$ .
  - Perform products of  $\tilde{\mathbf{x}}^o$  with weight matrices  $\mathbf{W}^G \in \mathbb{R}^{4096 \times 11008}$  and  $\mathbf{W}^U \in \mathbb{R}^{4096 \times 11008}$  in parallel. The result  $\mathbf{x}^g \in \mathbb{R}^{11008}$  performs the dot-product with result  $\mathbf{x}^u \in \mathbb{R}^{11008}$  after SiLU function. The output performs the product with weight  $\mathbf{W}^D \in \mathbb{R}^{11008 \times 4096}$  as in (3). We then get  $\mathbf{x}^d \in \mathbb{R}^{4096}$ .
  - Finally, the result of  $\mathbf{x}^d + \mathbf{x}^o$  is fed into the output layer  $\mathbf{W}^H \in \mathbb{R}^{4096 \times 32000}$ , we get  $\mathbf{y} \in \mathbb{R}^{32000}$  and then feed it into the softmax function.

### B. Low-rank Structure

As described in Section III-A, the linear layers are major building blocks of the transformer network [1]. An input sample  $\mathbf{x} \in \mathbb{R}^n$  is multiplied by a weight matrix  $\mathbf{W} \in \mathbb{R}^{n \times n}$ , and the output  $\mathbf{y} \in \mathbb{R}^n$  can be represented as follows:

$$\mathbf{y} = \mathbf{W}\mathbf{x}. \quad (4)$$

Empirical study found that the linear layers are highly redundant [33], allowing us to replace  $\mathbf{W} \in \mathbb{R}^{n \times n}$  with two sublinear layers,  $\mathbf{A} \in \mathbb{R}^{r \times n}$  and  $\mathbf{B} \in \mathbb{R}^{n \times r}$  with  $r \ll n$ . Then, (4) becomes:

$$\mathbf{y} = \mathbf{B}\mathbf{A}\mathbf{x}. \quad (5)$$

Note that the layer size is reduced from  $n^2$  to  $2nr$ , while the number of multiplications is reduced from  $n^2$  to  $2nr$ , too.

As an example, we replace the weight matrices of Llama2-7B [2] with a low-rank structure with  $r = 512$ .  $\mathbf{W}^K$ ,  $\mathbf{W}^Q$ ,  $\mathbf{W}^V$ , and  $\mathbf{W}^O$  are replaced with a pair of low-rank matrices  $\mathbf{A} \in \mathbb{R}^{4096 \times 512}$  and  $\mathbf{B} \in \mathbb{R}^{512 \times 4096}$ , respectively. The parameters of each weight matrix are reduced from 16.78 M to 4.19 M, and the total parameters of these weight matrices in the model are reduced from 2.15 B to 0.54 B.  $\mathbf{W}^U$  and  $\mathbf{W}^G$  are replaced with a pair of low-rank matrices  $\mathbf{A} \in \mathbb{R}^{4096 \times 512}$  and  $\mathbf{B} \in \mathbb{R}^{512 \times 11008}$ , respectively, and  $\mathbf{W}^D$  is replaced with a pair of low-rank matrices  $\mathbf{A} \in \mathbb{R}^{11008 \times 512}$  and  $\mathbf{B} \in \mathbb{R}^{512 \times 4096}$ . The parameters of each weight matrix are reduced from 45.09 M to 7.73 M, and the total parameters of these weight matrices in the model are reduced from 4.33 B to 0.74 B. Similarly, the parameters of  $\mathbf{W}^E$  and  $\mathbf{W}^H$  can be reduced from 262.14 M to 18.48 M, using such a low-rank structure.

### C. Challenges in Training and Inference

1) *Challenges in Training*: LLMs have a large number of parameters and usually take a long training time, as given in Table I. Pretraining an LLM has three primary challenges:

- Large scale dataset is needed to pretrain LLMs. For example, the dataset used to pretrain Llama2 [2] is 4.7

TABLE III  
BREAKDOWN OF GPU MEMORY FOOTPRINT FOR TRAINING LLAMA2-7B [2] AND LLAMA2-70B [2] WITH DIFFERENT BATCH SIZES.

LLMs	Batch size	Para. (GB)	Grad. (GB)	Opt. (GB)	Inter. (GB)
7B	1	14	14	84	81
	4	14	14	84	388
	16	14	14	84	1552
70B	1	140	140	840	442.5
	4	140	140	840	1770
	16	140	140	840	7080

TB, which requires large amounts of GPU and CPU memory.

- The memory footprint of pretraining and finetuning exceeds the GPU memory capacity. The GPU memory footprint can be classified into four parts, as shown in Table III. For pretraining Llama2-7B and Llama2-70B with batch size 16, the GPU memory footprint has a size of 1,664 GB and 8200 GB, respectively.
- In the model-parallel method, an LLM is split over multiple GPUs. During the pretraining, the forward pass is computed layer by layer and only one GPU is working at a time. When splitting an LLM into  $N$  GPUs, each GPU has a utilization of  $\frac{1}{N}$ , which is relatively low.

2) *Challenges in Inference*: During inference, we load the trained LLM into GPU. Using a standard tokenizer, the input text is processed into a sequence of tokens,  $\mathbf{X} \in \mathbb{R}^{l \times l}$ , where  $l$  is the sequence length and  $t$  is the vocabulary size. The input  $\mathbf{X}$  is then embedded into  $\mathbf{X}^e \in \mathbb{R}^{n \times l}$ . For  $h$  heads in multi-head self-attention module, there is an attention function in (1). This function uses  $\mathbf{K}_i, \mathbf{Q}_i, \mathbf{V}_i \in \mathbb{R}^{\frac{n}{h} \times l}$  to calculate attention score  $\text{softmax}(\frac{\mathbf{Q}_i \mathbf{K}_i^T}{\sqrt{d}}) \in \mathbb{R}^{l \times l}$  and  $head_i = \text{softmax}(\frac{\mathbf{Q}_i \mathbf{K}_i^T}{\sqrt{d}}) \mathbf{V}_i \in \mathbb{R}^{\frac{n}{h} \times l}$ ,  $i = 1, 2, \dots, h$ . Concatenating these heads, we get the  $s \in \mathbb{R}^{n \times l}$  in Fig. 2 to continue the process as Section III-A. Finally, the last column  $\mathbf{y} \in \mathbb{R}^t$  of output  $\mathbf{Y} \in \mathbb{R}^{t \times l}$  is the predicted token.

The inference stage has challenges as follows:

- Limited memory capacity poses a challenge in using LLMs for various applications, such as inference on mobile phones. For example, Llama2-7B has a size of 14 GB as shown in Table III. Using the low-rank structure with  $r = 512$ , the model has about 2 billion parameters, which has a size of 4 GB. It is still too large for mobile phones.
- As shown in Fig. 2, most parameters of the transformer structure come from the linear layers (4). In the inference stage, each parameter requires two operations, multiplication and addition. Therefore, Llama2-7B has a computational workload of 14 GFLOPS for each token. For generative LLM, each generated token needs an inference, that token is added to the end of input tokens as a new input for the next inference. For example, if the input has 100 tokens and the LLM generates 100 tokens, there are 100 times inference processes, these pro-

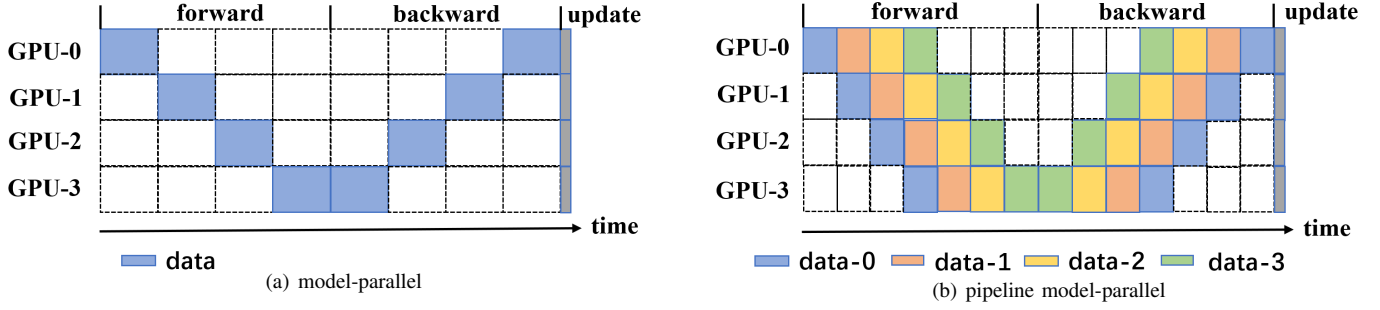


Fig. 3. Model-parallel and pipeline model-parallel methods.

cesses have 100, 101, ..., 199 tokens as input, respectively. Therefore, the whole inference stage has 14950 tokens to be computed. The computational workload of Llama2-7B is 210 TFLOPS. However, the mobile phone has a computational power of about 2 TFLOPs, and it will take 105 seconds which does not satisfy the requirement.

#### IV. PRETRAINING QUANTIZED LLMs USING LOW-RANK STRUCTURE

##### A. Pretraining Methods with Low-rank Structure

Pretraining an LLM has high costs and long training time. We replace the linear layers in the LLM with low-rank structure to reduce the number of parameters. For example, the  $\mathbf{W}^K \in \mathbb{R}^{4096 \times 4096}$  in Llama-7B can be replaced with two sub-linear layers, which have weight matrices of  $\mathbf{A}^K \in \mathbb{R}^{4096 \times r}$  and  $\mathbf{B}^K \in \mathbb{R}^{r \times 4096}$ . The parameters of this layer are reduced by  $\frac{4096}{2r}$ . Using a low-rank structure, we do the pretraining of LLMs as follows.

1) We replace a linear layer of the transformer with two sub-linear layers, which use a hidden layer with a small width, as shown in Fig. 1(a). In particular, a weight matrix  $\mathbf{W} \in \mathbb{R}^{n \times n}$  in Table II is replaced with two matrices,  $\mathbf{A} \in \mathbb{R}^{n \times r}$  and  $\mathbf{B} \in \mathbb{R}^{r \times n}$ . We refer to this as Method 1.

2) We decompose the pretrained weight matrix  $\mathbf{W} \in \mathbb{R}^{n \times n}$  in Table II into low-rank matrices  $\mathbf{A} \in \mathbb{R}^{n \times r}$  and  $\mathbf{B} \in \mathbb{R}^{r \times n}$ , as shown in Fig. 1(b). Then, we use  $\mathbf{A}$  and  $\mathbf{B}$  to initialize a low-rank LLM. We refer to this as Method 2.

3) Adding two narrow linear layers to the parallel path of the pretrained linear layer, we obtain the new linear layers as follows:

$$\mathbf{y} = \alpha \mathbf{W} \mathbf{x} + (1 - \alpha) \mathbf{B} \mathbf{A} \mathbf{x}, \quad 0 \leq \alpha \leq 1. \quad (6)$$

The pretrained linear  $\mathbf{W} \in \mathbb{R}^{n \times n}$  are frozen. At the beginning of pretraining,  $\alpha$  is set close to 1. Then,  $\alpha$  is decreased during the pretraining, until it is 0. The pretrained LLM has only the low-rank matrices  $\mathbf{A} \in \mathbb{R}^{n \times r}$  and  $\mathbf{B} \in \mathbb{R}^{r \times n}$ .

##### B. Optimization for the Pretraining Stage

We use low-rank LLMs in the pretraining stage. There are some challenges, as mentioned in Section III-C1, to be addressed.

TABLE IV  
GPU MEMORY CONSUMPTION OF INTERMEDIATE VARIABLES.

variables	#Parameters	Size (GB)
$x^e$	16.8 M	$\ll 0.1$
$\tilde{x}^e$	536,9 M	1.1
$k$	536,9 M	1.1
$q$	536,9 M	1.1
$v$	536,9 M	1.1
$qk^T$	17.2 B	34.4
$s$	17.2 B	34.4
$x^o$	536,9 M	1.1
$\tilde{x}^o$	536,9 M	1.1
$x^u$	1,4 B	2.8
$x^g$	1.4 B	2.8
$x^d$	536,9 M	$\ll 0.1$

##### Recomputing technique to avoid storing intermediate variables:

Intermediate variables are generated in the forward pass, used in backward pass, and then released. Table IV shows the GPU memory consumption of intermediate variables during the pretraining of Llama2-7B. The dimension, number of heads, batch size, and sequence length are 4096, 32, 1, and 4096, respectively.

Compared  $x^e$  with  $x^d$ , other intermediate variables have more GPU memory consumption. There are two reasons: 1) other variables are in the decoder layer, which has 32 layers. 2) Some variables,  $qk^T$ ,  $s$ , have the same size as  $k$ ,  $q$ ,  $v$  for each head. There are  $h = 32$  heads for each decoder layer.

By avoiding storing intermediate variables and recomputing them when needed, the GPU memory consumption can be significantly reduced, at the cost of more computations. The process of this method is as follows:

- 1) In forward pass, only the input, as  $x^e$ , is stored.
- 2) In backward pass, the GPU recomputes other variables using  $x^e$  for a decoder layer.
- 3) Calculating the gradients of parameters in this decoder layer, the variables are deleted after obtaining gradients.
- 4) Repeat steps 1) - 2) until all decoder layers calculate the gradients.
- 5) Obtaining all gradients, and the parameters are updated.

In this method, the peak memory consumption is the size of intermediate variables in one decoder layer. The GPU memory consumption is reduced from 81 GB to 2.5 GB, as in Table IV, at a cost of computational workload for an extra forward pass. We know that the computational workload of forward pass is half of backward pass. Therefore, the GPU memory consumption of intermediate variables can be reduced by 97% with a 33% increase in computation.

As shown in Table IV, these intermediate variables have different sizes. By selectively choosing which intermediate variables to recompute, there is a good balance between memory consumption and computation. For example,  $qk^T$  and  $s$  are much bigger than other variables. By only recomputing  $qk^T$  and  $s$ , we can reduce the GPU memory consumption from 81 GB to 12.2 GB, at the cost of about 6% increases in computation.

**Pipeline model-parallel method.** For pretraining an LLM on  $N$  GPUs, the model-parallel method loads the parameters on different GPUs, as shown in Fig. 3(a). The computing is performed sequentially on these GPUs, and each GPU has a utilization of  $\frac{1}{N}$ . In the pipeline model-parallel method, the input data is split into  $M \geq 1$  mini-batches. As shown in Fig. 3(b), we input these mini-batches into GPU-0 to GPU-3 sequentially and perform the backward pass in a reverse order. Then, the parameters are updated. In this method, the GPU has a utilization of  $\frac{M}{N+M-1}$ , where  $M \geq 1$ .

**Weight decomposition in parallel:** Decomposing weight  $W$  at different linear layers is independent. For example, Llama2-7B has 32 decoder layers, and each decoder layer has 7 linear layers as shown in Fig. 2. The decomposition stage has a parallelism of  $224 = 7 \times 32$ . In this method, we distribute the LLM decoder layers evenly across multiple GPUs. For example, the  $W^K$  in different decoder layers have the same size. In a single GPU, we batch the decomposition of these  $W^K$  in different layers. On different GPUs, we perform the decomposition of different weight matrices, such as  $W^Q$  and  $W^V$ , in parallel.

### C. Optimization for the Inference Stage

Utilizing the low-rank structure of the weights, the number of parameters of GPT2-1.5B can be reduced from 1.56 B to 0.59 B. This in turn can reduce the model size from 3.12 GB to 1.18 GB. By quantizing into 8-bit or 4-bit precision, the model will have a size of less than 0.59 GB, and thus can be loaded in mobile phones.

As described in Section III-B, the number of parameters of Llama2-7B can be reduced from 6.74 B to 1.32 B. For inputs and outputs that have 100 tokens in the inference stage as in Section III-C2, our method can reduce the computational workload from 210 to 40 TFLOPS and thus reduce the response time from about 105 to 20 seconds.

TABLE V  
THE PERFORMANCE AT DIFFERENT PRECISIONS.

Precision	Performance (TFLOPS)
FP32	19.5
FP16	312
int8	624
int4	1248

## V. FINETUNING QUANTIZED LLMs USING LOW-RANK STRUCTURE

### A. Our Finetuning Method

Many ongoing efforts are on finetuning pretrained models to obtain domain-specific LLMs. Compared with pre-training, fine-tuning of LLMs requires data of a much smaller scale. Low-rank adaptation (LoRA) method [4] provides a low-cost finetuning solution for LLMs, as shown in Fig. 5. This method finetunes a pretrained LLM on a domain-specific dataset. The finetuned LLM gains knowledge of the specific domain.

Given a pretrained LLM with weight  $W$ , the LoRA method adapts it to  $W' = W + \Delta W$  by adding a low-rank  $\Delta W = BA$ . The idea of the LoRA method [4] is as follows:

$$W'x = (W + \Delta W)x = Wx + BAx, \quad (7)$$

where  $W \in \mathbb{R}^{n \times n}$ ,  $A \in \mathbb{R}^{r \times n}$ ,  $B \in \mathbb{R}^{n \times r}$ ,  $r \ll n$ .

During the finetuning stage, the weight  $W$  is frozen, and the low-rank matrices  $A$  and  $B$  are trainable. In the inference stage, matrices product is performed with  $A$  and  $B$  and adding the result  $\Delta W$  to the pretrained weight  $W$ , which is denoted as  $W'$ .

### B. Optimization for the Finetuning Stage

**Quantization:** The low-rank adaptation method significantly reduces the number of trainable parameters. However, the pretrained weights have a larger memory consumption. For example, the pretrained weights of Llama2-7B [2] consume 14 GB of GPU memory during finetuning. In our method, the pretrained weights are quantized to lower precision. Low-precision data has a smaller size and is better suited for computing using GPU tensor cores, as shown in Table V. The pretrained weights of LLMs are in matrix form. We quantize the weights on per-vector as follows:

- The pretrained weight  $W \in \mathbb{R}^{n \times n}$  has  $n$  vectors, calculating the difference between the maximum and minimum values to get the scaling factor of each vector.
- In each vector, there are  $n$  elements multiplied with scaling factor. These multiplications are batched by mapping onto  $n$  CUDA cores.
- Results are stored in low-precision formats in GPU memory, while the original weights are deleted.

In quantization, there is a trade-off between memory footprint and accuracy with 8-bit and 8-bit data formats. These two data formats can reduce the GPU memory footprint of the

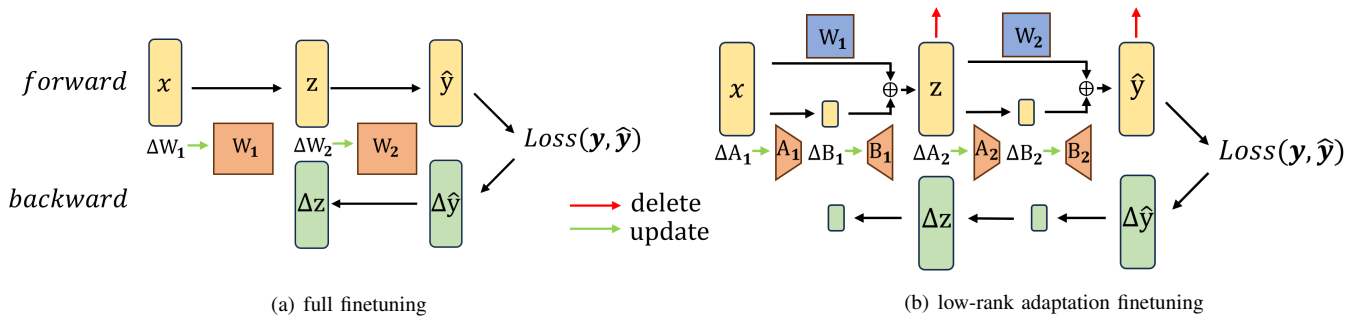


Fig. 4. Finetuning flow of low-rank adaptation method.

pretrained weights from 14 GB to 8 GB and 5 GB, respectively.

**Intermediate variables:** As shown in Fig. 4, the low-rank structure can reduce the trainable parameters from  $W_1$  to  $A_1$  and  $B_1$ . However, the intermediate variables, such as  $x, z$  and  $\hat{y}$ , for low-rank finetuning have the same size as full finetuning. We recompute the intermediate variables as in Section IV-B.

### C. Optimization for the Inference Stage

There is a growing interest in customized LLMs that are tailored to different scenarios or applications. In our method, we can view each customized model as a set of finetuned low-rank matrices  $A$  and  $B$ , sharing the base pretrained model  $W$ . The low-rank matrices have much fewer parameters, about 0.1% of that of the base model. There are two benefits:

- The storage can be significantly reduced for each customized LLM.
- By loading a base model with different finetuned low-rank matrices, the LLM can be used for different inference scenarios.

As described in Section III-C2, each generated token is added at the end of input sequence. Multiple tokens are calculated multiple times in inference stage. For example, the original input sequence has 100 tokens and the LLM generates 10 tokens. The original 100 tokens are input into LLM 10 times for inference. In our method, we store  $K, V \in \mathbb{R}^{n \times l}$  of each layer, as shown in Fig. 2. For each generated token, we input it into LLM to calculate  $\hat{q}, \hat{k}, \hat{v} \in \mathbb{R}^n$ . Then concatenating  $\hat{k}, \hat{v}$  with  $K, V$ , respectively. We cache the updated  $K, V \in \mathbb{R}^{n \times (l+1)}$ . Using this method, we can reduce the number of input tokens from  $l$  to 1, which can significantly reduce the computing workload in inference by  $l \times$ .

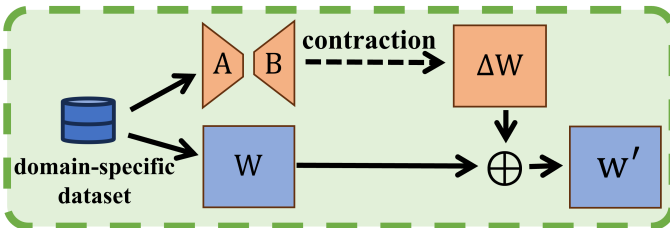


Fig. 5. The low-rank adaptation method for finetuning.

The cache of  $K, V$  have a huge block of GPU memory, which varies with the length of input sequence. There is a memory fragmentation problem, leading to inefficient use of GPU memory. PagedAttention [34] provides a method that refers to the virtual memory technique, splitting the  $K, V$  cache into multiple GPU blocks. There is a table mapping the logical cache and physical memory blocks.

## VI. PERFORMANCE EVALUATION

### A. Experimental Settings

**Server:** Our experiments were conducted on a DGX-2 server, equipped with two 64-core AMD EPYC 7742 CPUs, 8 NVIDIA A100 GPUs, and 2 TB of memory. The server was running Ubuntu 20.04 with CUDA 11.6, and we utilized PyTorch version 1.13 as our neural network framework.

#### Datasets, Baselines, and Metrics

**Training datasets.** We use the OpenWebText [35] dataset as our pretraining dataset. It is a clone of the GPT-2 WebText dataset and has about 11.2 B tokens. We use the alpaca dataset [36] and FinGPT dataset [37] for our finetuning method. The alpaca dataset was constructed using the self-instruct method and the FinGPT dataset was collected from financial websites. It contains 52K instruction-following examples.

**Evaluation datasets.** We evaluate our methods on two types of tasks: general tasks and financial tasks. The general tasks used the following three datasets:

- **BoolQ** [38] is a question answering dataset. It has 16K examples, and each example consists of a passage, question, and answer. The question is about the passage, and the answer is yes or no.
- **PIQA** [39] is a dataset about physical commonsense reasoning. It has 21K examples, and each example consists of a question and two possible solutions. The model to be evaluated needs to choose the most appropriate solution.
- **WinoGrande** [40] is a commonsense reasoning dataset. It has 44K sentences, and each sentence has a blank to be filled. The model to be evaluated needs to choose the correct one from the given two options.

The financial tasks used the following three datasets:

- **FPB** [41] consists of 4.8K sentences from financial news categorised by sentiment. Any news that may have a benefit or risk impact on investors is categorized as

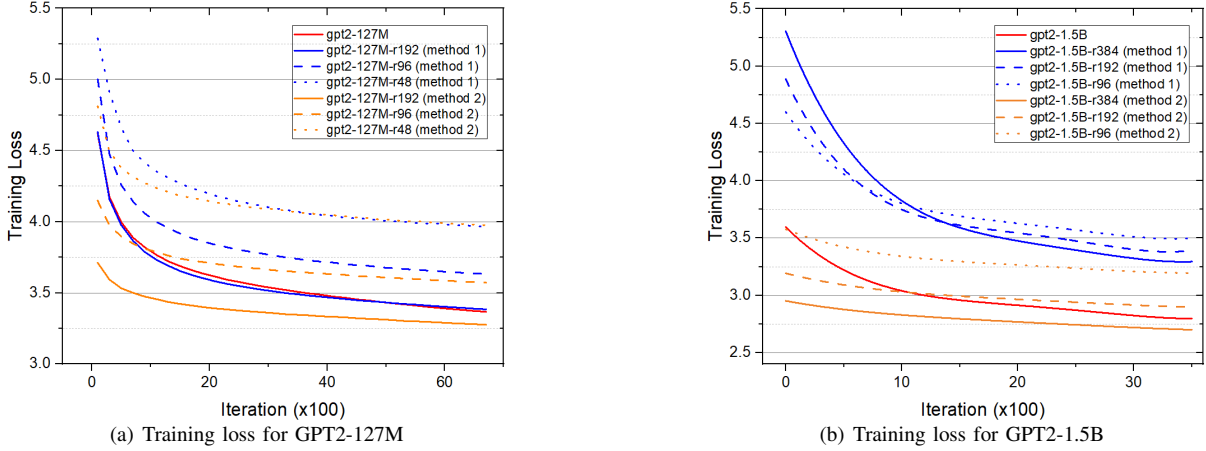


Fig. 6. Training loss for pretraining GPT2-127M and GPT2-1.5B using method 1 and method 2.

positive or negative. Other news that has no such effect is categorized as neutral.

- **FiQA SA** [42] consists of 17K sentences from microblog headlines and financial news. These sentences are classified according to sentiment as the FPB dataset.
- **TFNS** [43] consists of 11.9K sentences from annotated corpus of finance-related tweets. This dataset is used to classify finance-related tweets based on their sentiment.
- **NER** [44] consist of 1.4K sentences from financial agreements. This dataset is used to recognize the named entity.

We use GPT2-127M [11], GPT2-1.5B [11], Llama2-7B [2] and Llama2-13B [2] as our base LLMs.

- GPT2-127M [11] has 127M parameters. It contains  $N = 12$  layers with  $n = 786$  and  $h = 12$ .
- GPT2-1.5B [11] has 1.5B parameters. It contains  $N = 48$  layers with  $n = 1600$  and  $h = 25$ .
- Llama2-7B [2] has 6.7B parameters. It contains  $N = 32$  layers with  $n = 4096$  and  $h = 32$ .
- Llama2-13B [2] has 13B parameters. It contains  $N = 40$  layers with  $n = 5120$  and  $h = 40$ .

We show the F1 weighted scores for these tasks. For high-performance computing, we are interested in the following performance metrics:

- **Trainable parameters:** We are interested in the number of trainable parameters. These parameters will vary during finetuning.
- **GPU memory footprint:** We accumulate the GPU memory usage of all GPUs used for finetuning.
- **Training Time:** Time defined as (the number of GPUs used)  $\times$  (the process running time).

### B. Results for Pretraining LLMs Using Low-rank Structures

We use the GPT2-127M [11] and GPT2-1.5B [11] as the base LLM. We replace all weight matrices in Table II with low-rank structure, except for  $W^E$ . For GPT2-127M, we set rank  $r = 192, 96, 48$ , respectively; For GPT2-1.5B, we set rank  $r = 384, 192, 96$ , respectively. We pretrain our LLMs on

the OpenWebText dataset using method 1 and method 2 in Section IV-A. We evaluate them on general tasks.

For method 1 and method 2 as in Section IV-A, the training losses over training iterations are shown in Fig. 6. For GPT2-127M and GPT2-1.5B, our GPT2-127M-r192 (method 2) and GPT2-1.5B-r384 (method 2) have smaller loss values. For each model, the training loss of method 2 converges faster than method 1.

Table VI reports the testing accuracy, number of parameters, model size (8-bit), GPU memory footprint and training times for pretraining using method 1. For GPT2-127M, our method GPT2-127M-r192 achieves an accuracy increase of 0.8% and 1.8% on PIQA and WinoGrande,  $1.64\times$  compression ratio, and speedup of  $1.14\times$  in training time; For GPT2-1.5B, our method GPT2-1.5B-r384 achieves an accuracy increase of 0.2% on WinoGrande,  $2.64\times$  compression ratio, and speedup of  $1.31\times$  in training time.

Table VII reports the testing accuracy, number of parameters, model size (8-bit), GPU memory footprint and training times for pretraining using method 2. For GPT2-127M, our method GPT2-127M-r192 achieves an accuracy increase of 2.0% and 1.3% on PIQA and WinoGrande,  $1.64\times$  compression ratio, and speedup of  $1.15\times$  in training time; For GPT2-1.5B, our method GPT2-1.5B-r384 achieves an accuracy increase of 0.8%, 1.5%, 5.0% on these three datasets,  $2.64\times$  compression ratio, and speedup of  $1.31\times$  in training time; Our method GPT2-1.5B-r96 achieves an accuracy increase of 1.5% on WinoGrande,  $7.43\times$  compression ratio, and speedup of  $1.37\times$  in training time.

**Inference performance.** During the inference, our two methods have the same performance.

For GPT2-127M [11], our methods, GPT2-127M-r192, GPT2-127M-r96 and GPT2-127M-r48, achieve speedup of  $1.2\times$  in inference time, from 0.06 seconds to 0.05 seconds. For GPT-1.5B, our methods, GPT2-1.5B-r384, GPT2-1.5B-r192, GPT2-1.5B-r96, achieve speedup of  $1.9\times$  in inference time, from 0.43 seconds to 0.23.

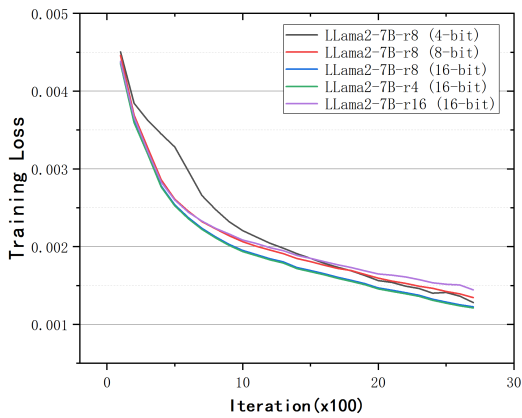


TABLE VI  
RESULT FOR PRETRAINING USING METHOD 1 IN FIG. 1.

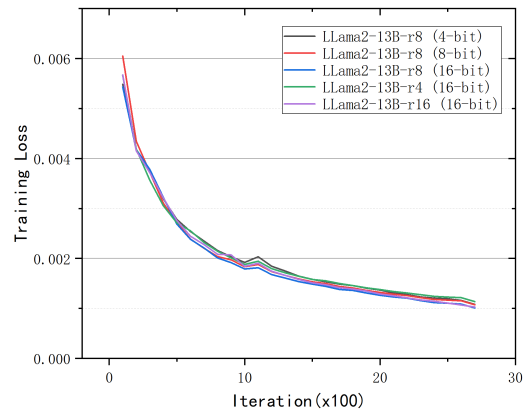
Model & Method	BoolQ	PIQA	WinoGrande	#Params. (Model size)	Memory (GB)	Time (hours)
GPT2-127M [11]	<b>61.9</b>	56.9	48.9	127.4 M (127.4 MB)	195.2	138.7
GPT2-127M-r192	48.1	<b>57.7</b>	50.7	77.5 M (77.5 MB)	192.4	121.0
GPT2-127M-r96	38.0	56.7	<b>51.3</b>	58.5 M (58.5 MB)	188.2	117.2
GPT2-127M-r48	51.8	55.8	50.0	49.0 M (49.0 MB)	187.6	116.4
GPT2-1.5B [11]	<b>59.9</b>	<b>63.6</b>	50.4	1.56 B (1.56 GB)	301.6	546.4
GPT2-1.5B-r384	58.5	58.7	<b>50.6</b>	0.59 B (0.59 GB)	238.0	416.3
GPT2-1.5B-r192	43.1	57.4	48.9	0.34 B (0.34 GB)	235.3	395.6
GPT2-1.5B-r96	43.7	57.2	49.5	0.21 B (0.21 GB)	264.0	399.6

TABLE VII  
RESULTS FOR PRETRAINING USING METHOD 2 IN FIG. 1.

Model & Method	BoolQ	PIQA	WinoGrande	#Params. (Model size)	Memory (GB)	Time (hours)
GPT2-127M [11]	<b>61.9</b>	56.9	48.9	127.4 M (127.4 MB)	195.2	138.7
GPT2-127M-r192	39.2	<b>58.9</b>	50.2	77.5 M (77.5 MB)	172.4	120.1
GPT2-127M-r96	47.8	55.7	<b>50.8</b>	58.5 M (58.5 MB)	196.1	116.9
GPT2-127M-r48	38.2	55.1	52.0	49.0 M (49.0 MB)	155.4	115.9
GPT2-1.5B [11]	59.9	63.6	50.4	1.56 B (1.56 GB)	301.6	546.4
GPT2-1.5B-r384	<b>60.7</b>	<b>65.9</b>	<b>55.4</b>	0.59 B (0.59 GB)	274.1	414.2
GPT2-1.5B-r192	46.7	62.4	51.5	0.34 B (0.34 GB)	275.8	401.9
GPT2-1.5B-r96	40.3	60.0	51.9	0.21 B (0.21 GB)	255.9	398.4



(a) Training loss for Llama2-7B



(b) Training loss for Llama2-13B

Fig. 7. Training loss for finetuning Llama2-7B, Llama2-13B with low-rank structure.

TABLE VIII  
RESULTS FOR FINETUNING IN FIG. 5.

Model & Method	BoolQ	PIQA	WinoGrande	FPB	FiQA SA	TFNS
Llama2-7B [2]	76.5	79.8	<b>70.1</b>	51.8	68.6	80.9
Llama2-7B-r8 (4-bit)	76.8	77.0	40.2	73.8	68.9	70.2
Llama2-7B-r8 (8-bit)	78.9	<b>81.8</b>	59.1	85.0	86.0	<b>89.4</b>
Llama2-7B-r8 (16-bit)	<b>82.8</b>	79.1	59.0	85.6	84.5	89.4
Llama2-7B-r4 (16-bit)	81.4	79.8	56.9	51.8	68.6	53.6
Llama2-7B-r16 (16-bit)	82.5	80.1	58.4	<b>86.4</b>	<b>86.8</b>	89.1
Llama2-13B [2]	74.2	72.3	<b>67.7</b>	54.2	73.0	63.1
Llama2-13B-r8 (4-bit)	84.6	83.0	63.0	70.1	69.2	73.0
Llama2-13B-r8 (8-bit)	84.7	83.2	62.8	<b>87.7</b>	<b>88.6</b>	90.2
Llama2-13B-r8 (16-bit)	85.0	83.1	62.8	40.0	56.1	58.9
Llama2-13B-r4 (16-bit)	84.2	82.9	62.7	26.4	54.2	39.9
Llama2-13B-r16 (16-bit)	<b>86.1</b>	<b>83.9</b>	63.0	87.6	84.2	<b>90.4</b>

TABLE IX  
RESULTS FOR FINETUNING IN FIG. 5.

Model & Method	Finetuning			Inference	
	#Params	Memory (GB)	Time (hours)	Model Size (GB)	Time (seconds)
Llama2-7B [2]	6.7 B	112	184,320	13.4	0.21
Llama2-7B-r8 (4-bit)	4.2 M	11.8	7.8	5.1	0.23
Llama2-7B-r8 (8-bit)	4.2 M	14.2	4.7	7.9	0.13
Llama2-7B-r8 (16-bit)	4.2 M	20.3	3.3	13.4	0.21
Llama2-7B-r4 (16-bit)	2.1 M	20.3	4.0	13.4	0.21
Llama2-7B-r16 (16-bit)	8.4 M	24.3	2.5	13.4	0.21
Llama2-13B [2]	6.7 B	208	368,640	26.2	0.39
Llama2-13B-r8 (4-bit)	9.8 M	17.7	8.5	9.8	0.78
Llama2-13B-r8 (8-bit)	9.8 M	30.4	6.8	15.5	0.23
Llama2-13B-r8 (16-bit)	9.8 M	32.7	5.4	26.2	0.39
Llama2-13B-r4 (16-bit)	4.9 M	32.7	5.4	26.2	0.39
Llama2-13B-r16 (16-bit)	19.6 M	33.0	6.1	26.2	0.39

### C. Results for Finetuning LLM Using Low-rank Structure

We finetune Llama2-7B [2] and Llama2-13B [2]. The pretrained weights have a data precision of 16-bit. We finetune these LLMs with low-rank structures with rank= 4, 8, 16. For rank = 8, we quantize these pretrained weights in 4-bit and 8-bit data precision, respectively.

Fig. 7 shows the training losses over iterations for our finetuning methods. For both Llama2-7B and Llama2-13B, these methods have similar loss curves. For the Llama2-7B, the Llama2-7B-r8 (16-bit) method has the smallest loss. For the Llama2-13B, the Llama2-7B-r8 (16-bit) method has the

smallest loss.

Table VIII reports the testing results on general tasks and financial tasks. For Llama2-7B, our methods Llama2-7B-r8 (8-bit) and Llama2-7B-r16 (16-bit) achieve average accuracy increase of 8.7% and 11.8%, respectively; For Llama2-13B, our methods Llama2-13B-r8 (8-bit) and Llama2-13B-r16 (16-bit) achieve average accuracy increase of 15.5% and 15.1%, respectively.

Table IX reports the number of trainable parameters, GPU memory footprint and finetuning time. For Llama2-7B, our methods Llama2-7B-r8 (4-bit) and Llama2-7B-r8 (8-

bit) achieve a memory compression ratio of  $9.5\times$  and  $7.8\times$ , reduce the model size from 13.4 GB to 5.1 GB and 7.9 GB, respectively; For Llama2-13B, our method Llama2-13B-r8 (4-bit) and Llama2-7B-r8 (8-bit) achieve a memory compression ratio of  $11.8\times$  and  $6.8\times$ , reduce the model size from 26.2 GB to 9.8 GB and 15.5 GB, respectively.

## VII. CONCLUSION AND FUTURE WORK

In this paper, we proposed an efficient pretraining and finetuning method for financial LLMs with low-rank structure. By taking advantage of the intrinsic low-rank dimension of LLMs, we replaced the linear layer in the transformer structure with low-rank matrices. For pretraining, we presented two methods: directly pretraining a low-rank LLM and decomposing the pretrained weights with low-rank structure to initialize a low-rank LLM. For finetuning, we added two low-rank matrices to the parallel path of the pretrained linear layer. The pretrained weights are frozen and only the low-rank weights are trainable. To further reduce the GPU memory consumption, we quantized the pretraining weights during the finetuning. We tested the proposed low-rank structure for pretraining GPT-127M and GPT-1.5B, and for finetuning Llama2-7B and Llama2-13B. The results show that we can achieve a high model performance with improved memory reduction and training speedup.

In the future, we will extend the low-rank structure to larger LLMs, e.g., Llama2-70B. We plan to implement a library that can build LLMs with low-rank structure.

## REFERENCES

- [1] A. Vaswani, N. Shazeer, N. Parmar, J. Uszkoreit, L. Jones, A. N. Gomez, L. Kaiser, I. Polosukhin, Attention is all you need, *Advances in neural information processing systems* (2017) 30 (2017).
- [2] H. Touvron, L. Martin, K. Stone, P. Albert, A. Almahairi, Y. Babaei, N. Bashlykov, S. Batra, P. Bhargava, S. Bhosale, et al., Llama 2: Open foundation and fine-tuned chat models, arXiv preprint arXiv:2307.09288 (2023).
- [3] A. Krizhevsky, One weird trick for parallelizing convolutional neural networks, arXiv preprint arXiv:1404.5997 (2014).
- [4] E. J. Hu, P. Wallis, Z. Allen-Zhu, Y. Li, S. Wang, L. Wang, W. Chen, et al., LoRA: Low-rank adaptation of large language models, in: *International Conference on Learning Representations*, 2022.
- [5] T. Dettmers, A. Pagnoni, A. Holtzman, L. Zettlemoyer, Qlora: Efficient finetuning of quantized llms, arXiv preprint arXiv:2305.14314 (2023).
- [6] M. Xu, Y. L. Xu, D. P. Mandic, TensorGPT: Efficient compression of the embedding layer in LLMs based on the tensor-train decomposition, arXiv preprint arXiv:2307.00526 (2023).
- [7] T. Brown, B. Mann, N. Ryder, M. Subbiah, J. D. Kaplan, P. Dhariwal, A. Neelakantan, P. Shyam, G. Sastry, A. Askell, et al., Language models are few-shot learners, *Advances in Neural Information Processing Systems* 33 (2020) 1877–1901.
- [8] E. Almazrouei, H. Alobeidli, A. Alshamsi, A. Cappelli, R. Cojocaru, M. Debbah, E. Goffinet, D. Heslow, J. Launay, Q. Malartic, B. Noune, B. Pannier, G. Penedo, Falcon-40B: an open large language model with state-of-the-art performance (2023).
- [9] Z. Du, Y. Qian, X. Liu, M. Ding, J. Qiu, Z. Yang, J. Tang, Glm: General language model pretraining with autoregressive blank infilling, in: *Proceedings of the 60th Annual Meeting of the Association for Computational Linguistics (Volume 1: Long Papers)*, 2022, pp. 320–335.
- [10] A. Q. Jiang, A. Sablayrolles, A. Mensch, C. Bamford, D. S. Chaplot, D. d. I. Casas, F. Bressand, G. Lengyel, G. Lample, L. Saulnier, et al., Mistral 7B, arXiv preprint arXiv:2310.06825 (2023).
- [11] A. Radford, J. Wu, R. Child, D. Luan, D. Amodei, I. Sutskever, et al., Language models are unsupervised multitask learners, *OpenAI blog* 1 (8) (2019) 9.
- [12] A. Radford, K. Narasimhan, T. Salimans, I. Sutskever, et al., Improving language understanding by generative pre-training (2018).
- [13] L. Ouyang, J. Wu, X. Jiang, D. Almeida, C. Wainwright, P. Mishkin, C. Zhang, S. Agarwal, K. Slama, A. Ray, et al., Training language models to follow instructions with human feedback, *Advances in Neural Information Processing Systems* 35 (2022) 27730–27744.
- [14] H. Touvron, T. Lavril, G. Izacard, X. Martinet, M.-A. Lachaux, T. Lacroix, B. Rozière, N. Goyal, E. Hambro, F. Azhar, et al., LLaMA: Open and efficient foundation language models, arXiv preprint arXiv:2302.13971 (2023).
- [15] J. Kaplan, S. McCandlish, T. Henighan, T. B. Brown, B. Chess, R. Child, S. Gray, A. Radford, J. Wu, D. Amodei, Scaling laws for neural language models, arXiv preprint arXiv:2001.08361 (2020).
- [16] K. Cobbe, V. Kosaraju, M. Bavarian, M. Chen, H. Jun, L. Kaiser, M. Plappert, J. Tworek, J. Hilton, R. Nakano, et al., Training verifiers to solve math word problems, arXiv preprint arXiv:2110.14168 (2021).
- [17] J. Wei, Y. Tay, R. Bommasani, C. Raffel, B. Zoph, S. Borgeaud, D. Yogatama, M. Bosma, D. Zhou, D. Metzler, et al., Emergent abilities of large language models, arXiv preprint arXiv:2206.07682 (2022).
- [18] A. Novikov, D. Podoprikin, A. Osokin, D. P. Vetrov, Tensorizing neural networks, *Advances in Neural Information Processing Systems* 28 (2015).
- [19] K. Hayashi, T. Yamaguchi, Y. Sugawara, S.-i. Maeda, Exploring unexplored tensor network decompositions for convolutional neural networks, *Advances in Neural Information Processing Systems* 32 (2019).
- [20] T. Zhang, X.-Y. Liu, cutensor-tubal: Optimized gpu library for low-tubal-rank tensors, in: *ICASSP 2019-2019 IEEE International Conference on Acoustics, Speech and Signal Processing (ICASSP)*, IEEE, 2019, pp. 8583–8587.
- [21] H. Lu, T. Zhang, X.-Y. Liu, High-performance homomorphic matrix completion on gpus, in: *2019 IEEE 21st International Conference on High Performance Computing and Communications; IEEE 17th International Conference on Smart City; IEEE 5th International Conference on Data Science and Systems (HPCC/SmartCity/DSS)*, IEEE, 2019, pp. 1627–1634.
- [22] H. Li, T. Zhang, R. Zhang, X.-Y. Liu, High-performance tensor decoder on gpus for wireless camera networks in iot, in: *2019 IEEE 21st International Conference on High Performance Computing and Communications; IEEE 17th International Conference on Smart City; IEEE 5th International Conference on Data Science and Systems (HPC-C/SmartCity/DSS)*, IEEE, 2019, pp. 1619–1626.
- [23] T. Zhang, W. Kan, X.-Y. Liu, High performance gpu primitives for graph-tensor learning operations, *Journal of Parallel and Distributed Computing* 148 (2021) 125–137.
- [24] T. Zhang, X.-Y. Liu, X. Wang, A. Walid, cutensor-tubal: Efficient primitives for tubal-rank tensor learning operations on gpus, *IEEE Transactions on Parallel and Distributed Systems* 31 (3) (2019) 595–610.
- [25] T. Zhang, X.-Y. Liu, X. Wang, High performance gpu tensor completion with tubal-sampling pattern, *IEEE Transactions on Parallel and Distributed Systems* 31 (7) (2020) 1724–1739.
- [26] H. Huang, X.-Y. Liu, W. Tong, T. Zhang, A. Walid, X. Wang, High performance hierarchical tucker tensor learning using gpu tensor cores, *IEEE Transactions on Computers* (2022).
- [27] X.-Y. Liu, Z. Zhang, Z. Wang, H. Lu, X. Wang, A. Walid, High-performance tensor learning primitives using gpu tensor cores, *IEEE Transactions on Computers* (2022).
- [28] T. Dettmers, M. Lewis, Y. Belkada, L. Zettlemoyer, Gpt3. int8 (): 8-bit matrix multiplication for transformers at scale, *Advances in Neural Information Processing Systems* 35 (2022) 30318–30332.
- [29] T. Dettmers, M. Lewis, Y. Belkada, L. Zettlemoyer, Llm. int8 (): 8-bit matrix multiplication for transformers at scale, arXiv preprint arXiv:2208.07339 (2022).
- [30] G. Xiao, J. Lin, M. Seznec, H. Wu, J. Demouth, S. Han, Smoothquant: Accurate and efficient post-training quantization for large language models, in: *International Conference on Machine Learning*, PMLR, 2023, pp. 38087–38099.
- [31] E. Frantar, S. Ashkboos, T. Hoefler, D. Alistarh, Gptq: Accurate post-training quantization for generative pre-trained transformers, arXiv preprint arXiv:2210.17323 (2022).

- [32] J. Su, M. Ahmed, Y. Lu, S. Pan, W. Bo, Y. Liu, Roformer: Enhanced transformer with rotary position embedding, *Neurocomputing* 568 (2024) 127063.
- [33] Y. Cheng, F. X. Yu, R. S. Feris, S. Kumar, A. Choudhary, S.-F. Chang, An exploration of parameter redundancy in deep networks with circulant projections, in: *Proceedings of the IEEE International Conference on Computer Vision*, 2015, pp. 2857–2865.
- [34] W. Kwon, Z. Li, S. Zhuang, Y. Sheng, L. Zheng, C. H. Yu, J. Gonzalez, H. Zhang, I. Stoica, Efficient memory management for large language model serving with pagedattention, in: *Proceedings of the 29th Symposium on Operating Systems Principles*, 2023, pp. 611–626.
- [35] A. Gokaslan, V. Cohen, Openwebtext, <https://github.com/Skylion007/openwebtext> (2019).
- [36] R. Taori, I. Gulrajani, T. Zhang, Y. Dubois, X. Li, C. Guestrin, P. Liang, T. B. Hashimoto, Stanford alpaca: An instruction-following llama model (2023).
- [37] X.-Y. Liu, G. Wang, H. Yang, D. Zha, Data-centric FinGPT: Democratizing internet-scale data for financial large language models, *NeurIPS Workshop on Instruction Tuning and Instruction Following* (2023).
- [38] C. Clark, K. Lee, M.-W. Chang, T. Kwiatkowski, M. Collins, K. Toutanova, Boolq: Exploring the surprising difficulty of natural yes/no questions, in: *NAACL*, 2019.
- [39] Y. Bisk, R. Zellers, R. L. Bras, J. Gao, Y. Choi, Piqa: Reasoning about physical commonsense in natural language, in: *Thirty-Fourth AAAI Conference on Artificial Intelligence*, 2020.
- [40] Winogrande: An adversarial winograd schema challenge at scale, 2019.
- [41] P. Malo, A. Sinha, P. Korhonen, J. Wallenius, P. Takala, Good debt or bad debt: Detecting semantic orientations in economic texts, *Journal of the Association for Information Science and Technology* 65 (4) (2014) 782–796.
- [42] M. Maia, S. Handschuh, A. Freitas, B. Davis, A. Balahur, Wwv’18 open challenge: Financial opinion mining and question answering, in: *Companion of the The Web Conference 2018*, 2018.
- [43] N. Magic, Twitter financial news senti-ment, <http://precog.iiitd.edu.in/people/anupama>, (2022).
- [44] J. C. S. Alvarado, K. Verspoor, T. Baldwin, Domain adaption of named entity recognition to support credit risk assessment, in: *Proceedings of the Australasian Language Technology Association Workshop 2015*, 2015, pp. 84–90.